Nanoscale

Nondestructive, Longitudinal Measurement of Collagen Scaffold Degradation Using Computed Tomography and Gold Nanoparticles

Journal:	*Nanoscale*
Manuscript ID	NR-ART-01-2019-000313.R1
Article Type:	Paper
Date Submitted by the Author:	08-Feb-2019
Complete List of Authors:	Finamore, Tyler; University of Notre Dame, Aerospace and Mechanical Engineering, Bioengineering Graduate Program Curtis, Tyler; University of Notre Dame, Aerospace and Mechanical Engineering, Bioengineering Graduate Program Tedesco, James ; McMaster University, Department of Materials Science and Engineering; University of Notre Dame, Aerospace and Mechanical Engineering, Bioengineering Graduate Program Grandfield, Kathryn; McMaster University, Department of Materials Science and Engineering Roeder, Ryan; University of Notre Dame, Aerospace and Mechanical Engineering, Bioengineering Graduate Program

Nondestructive, Longitudinal Measurement of Collagen Scaffold Degradation Using Computed Tomography and Gold Nanoparticles

Tyler A. Finamore,[1] Tyler E. Curtis,[1] James V. Tedesco,[1,2]
Kathryn Grandfield,[2] and Ryan K. Roeder[1,3]

[1]Department of Aerospace and Mechanical Engineering
Bioengineering Graduate Program
University of Notre Dame
Notre Dame, IN 46556, USA

[2]Department of Materials Science and Engineering
McMaster University
Hamilton, ON L8S 4L8, Canada

[3]Notre Dame Center for Nanoscience and Nanotechnology (ND*nano*)
University of Notre Dame
Notre Dame, IN 46556, USA

Submitted to: *Nanoscale*

Keywords: collagen scaffolds, contrast agent, enzymatic degradation, drug delivery, gold nanoparticles, X-ray computed tomography

Correspondence: Ryan K. Roeder, Ph.D., Professor
Department of Aerospace and Mechanical Engineering
Bioengineering Graduate Program
148 Multidisciplinary Research Building
University of Notre Dame
Notre Dame, IN 46556

Phone: (574) 631-7003
Email: rroeder@nd.edu

Funding Sources: National Science Foundation (DMR-1309587)
International Precious Metals Institute
Kelly Cares Foundation
St. Joseph Health System

Abstract

Biodegradable materials, such as collagen scaffolds, are used extensively in clinical medicine for tissue regeneration and/or as an implantable drug delivery vehicle. However, available methods to study biomaterial degradation are typically invasive, destructive, and/or non-volumetric. Therefore, the objective of this study was to investigate a new method for nondestructive, longitudinal, and volumetric measurement of collagen scaffold degradation. Gold nanoparticles (Au NPs) were covalently conjugated to collagen fibrils during scaffold preparation to enable contrast-enhanced imaging of collagen scaffolds. The X-ray attenuation of as-prepared scaffolds increased linearly with increased Au NP concentration such that ≥ 60 mM Au NPs provided sufficient contrast to measure scaffold degradation. Collagen scaffold degradation kinetics were measured to increase during *in vitro* enzymatic degradation in media with an increased concentration of collagenase. The scaffold degradation kinetics measured by micro-CT exhibited lower variability compared with gravimetric measurement and were validated by measurement of the release of Au NPs from the same samples by optical spectroscopy. Thus, Au NPs and CT synergistically enabled nondestructive, longitudinal, and volumetric measurement of collagen scaffold degradation.

Introduction

Natural (e.g., collagen) and synthetic (e.g., polylactide-*co*-glycolide) polymers are used extensively in clinical medicine as scaffolds for tissue regeneration and/or implantable vehicles for drug delivery [1-3]. The biomaterial degradation rate is critical and often designed to match the rate of tissue regeneration and/or control the rate of drug release [4]. However, common methods for measuring biomaterial degradation *in vitro* or *in vivo*, such as gravimetric analysis [5-9], mechanical testing [5-8], molecular weight characterization by gel permeation chromatography [7-9], histology [8], and hydroxyproline assay [6,10], are destructive and invasive. Thus, *in vitro* measurements require multiple samples at multiple time points incubated in physiological media that may not recapitulate *in vivo* behavior, while *in vivo* measurements require excision of implants in multiple animals at multiple time points [5,8,9].

Non-invasive, longitudinal, and volumetric measurement of biomaterial degradation *in vivo* would be highly advantageous but remains uncommon. Noninvasive assessment of biomaterial degradation *in vivo* is possible with fluorescent labels and optical imaging systems [11-13], but is typically restricted to two-dimensional (2D) imaging and subcutaneous implants due to limited light transmission through tissue. Contrast-enhanced magnetic resonance imaging enables noninvasive, volumetric assessment of biomaterial degradation *in vivo* with high sensitivity [14-16], but is limited by availability and acquisition time [16]. Various acoustic imaging methods are also gaining interest [17-19], but have various limitations including 2D imaging, low spatial resolution, low tissue contrast, and tissue depth [16,19].

X-ray computed tomography (CT) provides high spatiotemporal resolution and deep tissue imaging, but has been limited to *in vitro* imaging of biomaterial degradation [20,21] due to low tissue contrast [16]. Biodegradable polymers and calcium phosphates exhibit similar X-ray attenuation as soft tissue and mineralized tissue, respectively. However, contrast-enhanced CT can be used to overcome this limitation [16], and was recently demonstrated for scaffolds comprising nanoparticles (NPs) physically entrapped within an agarose or alginate matrix [22]. NPs are advantageous in providing a greater mass per particle, and thus greater X-ray contrast, compared with small molecules and chelates, because X-ray contrast is primarily governed by the mass concentration of the contrast agent [23]. Importantly, gold (Au) NPs have become a widely investigated X-ray contrast agent in preclinical research, due to exhibiting high X-ray attenuation, biocompatibility, and facile surface functionalization for bioconjugation [23], which can be leveraged to covalently link Au NPs to protein-based scaffold biomaterials.

Therefore, the objective of this study was to investigate nondestructive, longitudinal, and volumetric measurement of collagen scaffold degradation by contrast-enhanced CT using Au NPs. Au NPs were surface functionalized with mercaptosuccinic acid (MSA) and covalently conjugated to type I collagen fibrils during scaffold fabrication (Fig. 1). The degradation kinetics of collagen scaffolds were measured longitudinally by contrast-enhanced micro-CT due to the release of Au NPs upon enzymatic degradation *in vitro*. Measurements by micro-CT were compared to measurements on the same samples by gravimetric analysis and optical spectroscopy.

Results and discussion

Collagen scaffold preparation and characterization

Au NPs were synthesized using the citrate reduction method, surface functionalized with MSA via Au-thiol bonding, and covalently conjugated to type I collagen fibrils via carboxyl-to-amine crosslinking using 1-ethyl-3-(3-dimethylaminopropyl)carbodiimide (EDC) and *n*-hydroxysuccinimide (NHS) (Fig. 1). Collagen scaffolds were subsequently prepared by condensing collagen fibrils conjugated with Au NPs, mixing with paraffin microspheres as a porogen, compression molding, leaching the porogen to create porosity, and crosslinking by EDC/NHS chemistry. The use of collagen fibrils modified by conjugation with Au NPs required no alterations to previously established methods for preparing cytocompatible collagen scaffolds [24,25]. Therefore, similar strategies are readily envisioned for conjugating Au NPs to other protein- and polysaccharide-based degradable biomaterials, such as albumin, alginate, chitosan, elastin, fibrin, and silk fibroin [26].

As-prepared collagen scaffolds exhibited a hierarchical structure with a microarchitecture comprising collagen struts and porosity (Fig. 2a). Scaffold porosity was uniformly distributed, spherical, and interconnected (Fig. 2a, 3a,b). The total scaffold porosity was measured by micro-CT to be ~90 and ~80% by volume in wet and dry scaffolds, respectively. Importantly, ~99% of the pore volume was interconnected. The mean (± standard deviation) pore diameter was measured by micro-CT as 280 (70) and 200 (70) μm in wet and dry scaffolds, respectively. Differences in the porosity and mean pore diameter between wet and dry scaffolds were due to scaffold shrinkage during critical point drying, and were consistent with previous reports [27,28].

The nanostructure of the collagen scaffold matrix comprised collagen fibrils and conjugated Au NPs (Fig. 2b,c). Au NPs were uniformly distributed throughout the overall scaffold, as evidenced by uniform X-ray contrast observed qualitatively in micro-CT (Fig. 2a, 3a), and within the collagen matrix, as evidenced in transmission electron microscopy (TEM) (Fig. 2b,c, 3c). Some agglomeration of Au NPs was evident but the majority were observed as individual NPs (Fig. 3d). The mean (± standard deviation) diameter of individual Au NPs in the collagen matrix was measured to be 15.7 (1.6) nm. Importantly, Au NPs were spatially associated with collagen fibrils (Fig. 2b) and not the space in between collagen fibrils. This observation suggests that Au

NPs were covalently conjugated to collagen fibrils and not merely trapped in between collagen fibrils during scaffold preparation.

Collagen scaffolds were prepared with varying concentrations of Au NPs to determine a suitable concentration for contrast-enhanced micro-CT (Fig. 4). The X-ray attenuation of collagen scaffolds increased linearly with Au NP concentration ($p < 0.0001$), as expected, and was strongly correlated ($R^2 = 0.95$). Scaffolds containing at least 60 mM Au NPs exhibited significantly greater X-ray attenuation compared with phosphate buffered saline (PBS) ($p < 0.005$, *t*-test vs. 58 HU), which exhibits X-ray attenuation comparable to that of soft tissue, and reached ~1000 HU with 80 mM Au NPs (Fig. 4). Thus, the X-ray contrast of collagen scaffolds was able to be tuned by increasing the concentration of Au NPs in the scaffold.

Based on these results, collagen scaffolds were prepared with 80 mM Au NPs for subsequent enzymatic degradation experiments in order to retain sufficient contrast for detection and quantification over the entire time course of complete enzymatic degradation. Concentrations greater than 80 mM Au NPs could be expected to provide even greater X-ray contrast, and could be necessary for contrast-enhanced imaging of biocomposite scaffolds containing calcium phosphate fillers or adjacent to bone. However, beam hardening may also become more prominent with greater than 80 mM Au NPs, resulting in a greater possibility of imaging artifacts and thus error in measuring the segmented scaffold volume [29].

Collagen scaffold degradation kinetics

Collagen scaffold degradation kinetics were measured longitudinally in media containing 0, 0.3, and 0.5 mg/ml collagenase by the segmented scaffold volume using contrast-enhanced micro-CT, the cumulative release of Au NPs into the media using inductively-coupled plasma optical emission spectroscopy (ICP-OES), and the scaffold mass using gravimetric analysis (Fig. 5).

Collagen scaffolds exhibited no measurable degradation (Fig. 5a,c), and minimal (~5 %) release of Au NPs (Fig. 5b), over 9 days in the absence of collagenase. These results confirmed that collagen fibrils were covalently crosslinked and that Au NPs were covalently conjugated to collagen fibrils. The scaffold degradation kinetics increased with an increase in collagenase concentration (Fig. 5, $p < 0.0001$, GLM), as expected. The scaffold degradation kinetics were modeled using a three-parameter logistic equation (Table 1). Increased collagenase concentration resulted in a decreased degradation half-life (t_{50}), increased growth rate parameter (a), and decreased inflection point (b).

The collagen scaffold degradation kinetics measured by micro-CT were compared with measurements by ICP-OES and gravimetric analysis on the same specimens. Both micro-CT and ICP-OES measurements exhibited similar variability, which was significantly lower than that for gravimetric analysis (Fig. 5, Table 1). Overall, differences between measurement methods were not statistically significant ($p = 0.48$, GLM). However, the degradation half-life measured by ICP-OES was 11 and 23% greater than that measured by micro-CT for a collagenase concentration of 0.3 and 0.5 mg/ml, respectively (Table 1) . It is not surprising that the scaffold volume and mass decreased more rapidly than Au NPs were released from the scaffold considering that the scaffold and/or scaffold fragments had to be collected by centrifugation at each time prior to imaging. Therefore, these results verified that enzymatic degradation of collagen scaffolds was accompanied by the release of Au NPs into the supernatant media. These results also suggest that micro-CT measurements of the scaffold degradation kinetics were more precise compared with gravimetric analysis and were validated by ICP-OES.

Micro-CT images were acquired at relatively low spatial resolution (100 μm voxel size) in order to replicate *in vivo* imaging, which did not permit segmentation of the scaffold microarchitecture (Fig. 5a). Instead, the entire scaffold volume was segmented from surrounding media, as is common for *in vivo* imaging, for contrast-enhanced micro-CT measurements of scaffold degradation *in vitro* (Fig. 5a). However, even this may not always be practical or feasible for longitudinal *in vivo* imaging. Therefore, scaffold degradation was also measured by the mean X-ray attenuation within a fixed, overall volume of interest (VOI) to further replicate possible *in vivo* imaging methods. The mean X-ray attenuation measured by micro-CT within the fixed, overall VOI decreased linearly and was strongly correlated ($R^2 = 0.84$) with the cumulative degradation determined from the segmented scaffold volume in micro-CT (Fig. 6). This result suggests that measurements of the mean X-ray attenuation within a fixed VOI can serve a suitable surrogate for the segmented scaffold volume if necessary when imaging *in vivo*, even when the selected VOI is larger than the actual scaffold volume.

Limitations and opportunities

Au NPs were a logical choice for the contrast agent in this study, due to exhibiting high X-ray attenuation, biocompatibility, and facile surface functionalization for bioconjugation [23]. Au NPs may also be encapsulated with a silica shell loaded with fluorophores to enable bimodal imaging by fluorescence and CT [30]. Other NP contrast agents with multifunctional capabilities [31-33] may also be utilized provided the surface chemistry is amenable to molecular functionalization with appropriate ligands for crosslinking to the biomaterial. Importantly, collagen scaffolds and extracellular matrix conjugated with Au NPs were previously shown to exhibit cytocompatibility as good or better than crosslinked collagen scaffolds alone [34,35]. Moreover, Au NPs of comparable size, surface functionalization, and dose were readily cleared from soft tissues in mice within 1-2 days after administration and were accumulated primarily in the liver and spleen with no evidence of cytotoxicity for up to 28 days after administration [36]. Therefore, these studies suggest that Au NPs are well-suited for use *in vivo* but also indicate a need for careful experimental design to account for any concomitant effect of the NP contrast agent and its clearance on the behavior under investigation.

The *in vitro* model of enzymatic collagen scaffold degradation demonstrated the feasibility of nondestructive, longitudinal, and volumetric measurement of collagen scaffold degradation by contrast-enhanced CT using conjugated Au NPs, and further suggested potential utility for non-invasive, *in vivo* imaging. However, this model was only intended to recapitulate plausible *in vivo* behavior for proof-of-concept and was not intended to fully recapitulate *in vivo* degradation kinetics and mechanisms. For example, the scaffold degradation rate in this study was highly accelerated; collagen scaffolds lacking conjugated Au NPs, but otherwise identical to those in this study, were not yet fully degraded after 12 weeks subcutaneous implantation in mice [25].

Further work is therefore required to demonstrate this new method in an *in vivo* model of scaffold degradation, such as subcutaneous ectopic [5,10-13,25,37], intramuscular ectopic [11,12,38,39] or orthotopic [8,39-41] animal models. Moreover, further work is also required to determine if conjugated Au NPs can enable contrast-enhanced imaging of the degradation of biomaterials which also contain X-ray attenuating calcium phosphate fillers or invading calcified tissue. In this case, emerging multi-energy CT imaging techniques can enable discrimination and quantification of the calcium phosphate fillers or calcified tissues versus contrast agents even when spatially coincident [42]. Last, further work is required to determine if the minimal (~5 %) release of Au NPs (Fig. 5b) observed in the absence of collagenase was due to degradation of collagen scaffolds that was below the measurement sensitivity of micro-CT or the passive release of non-conjugated Au NPs.

In summary, contrast-enhanced CT enabled nondestructive, longitudinal, and volumetric measurement of the degradation kinetics of a low-attenuating biomaterial (e.g., natural or synthetic polymer), for the first time to our knowledge, by covalently conjugating Au NPs to the scaffold biomaterial such that the Au NPs were only released upon enzymatic degradation. Nondestructive and longitudinal measurements are highly advantageous to reduce the number samples and animals required to achieve sufficient statistical power. Noninvasive measurements are similarly highly advantageous to eliminate the need for excision of implanted biomaterials, but require further validation. Nonetheless, the results of this study suggest that contrast-enhanced micro-CT can provide a powerful new tool for studying the effects of molecular structure or composition [11,13,21], crosslinking treatments [6,10,43], cell seeding [37,41], and growth factor delivery [38-40], among other factors, on biomaterial degradation, as well as the effects of biomaterial degradation rate and/or drug release on tissue regeneration [7,8,38-41,44], in both *in vitro* and *in vivo* models. Over the last two decades, micro-CT imaging systems have becoming widely available and micro-CT imaging methods have become well-established [45]. Therefore, the approach demonstrated in this study provides a simple, widely-available, and useful tool which may be advantageous for preclinical research investigating tissue regeneration and drug delivery.

Conclusions

Au NPs were covalently conjugated to collagen scaffolds to enable nondestructive, longitudinal, and volumetric measurement of enzymatic degradation using contrast-enhanced micro-CT. The X-ray attenuation of as-prepared scaffolds increased linearly with increased Au NP concentration such that ≥ 60 mM Au NPs provided sufficient contrast to measure scaffold degradation. Collagen scaffold degradation kinetics were measured to increase during *in vitro* enzymatic degradation in media with an increased concentration of collagenase. The scaffold degradation kinetics measured by micro-CT exhibited lower variability compared with gravimetric measurement and were validated by measurement of the release of Au NPs from the same samples by optical spectroscopy. Thus, Au NPs and CT synergistically enabled nondestructive, longitudinal, and volumetric measurement of collagen scaffold degradation, which may be advantageous for preclinical research investigating tissue regeneration and drug delivery

Experimental methods

MSA-Au NP synthesis and characterization

Au NPs were prepared by the citrate reduction method using methods previously described in detail [46,47]. Briefly, 0.1 g gold (III) chloride trihydrate ($HAuCl_4 \cdot 3H_2O$, ≥99.9%, Sigma-Aldrich) was added to 500 mL deionized (DI) water and brought to a boil under stirring. Once boiling, 0.5 g sodium citrate ($C_6H_5Na_3O_7 \cdot 2H_2O$, ACS reagent, Sigma-Aldrich) was added. The solution was boiled for 20 min, removed from heat, stirred overnight, and readjusted to 500 mL after reaching ambient temperature. As-prepared Au NPs were surface-functionalized with mercaptosuccinic acid (MSA, $C_4H_6O_4S$, 97%, Sigma-Aldrich) by adding 15 mL of 10 mM MSA in DI water to 500 mL of 0.5 mM Au NPs [25]. MSA-functionalized Au NPs (MSA-Au NPs) were concentrated to ~50 mM by centrifugation at ~11,000*g* for 1 h. MSA-Au NPs were previously reported to exhibited a mean (±standard deviation) particle diameter of 13.2 (0.9) nm [47].

Collagen scaffold fabrication and conjugation

Collagen scaffolds were prepared by compression molding and porogen leaching, adapting previously established methods [24,25]. Bovine type I collagen (lyophilized fibrous powder, Advanced Biomatrix) was added to 25 mL of DI water at a concentration of 4 mg/ml. MSA-Au NPs were added to the collagen solution in amounts calculated to yield a Au concentration of 0, 20, 40, 60, or 80 mM within the final total scaffold volume, assuming a density of 1.23 g/cm^3 for condensed collagen [48] and 0.8 g/cm^3 for the paraffin porogen, and homogenized (Polytron PT 2100, Kinematica AG) at 19,000 rpm for 10 min. Note that for scaffolds comprising 80 mM Au NPs, 15.8 mg Au NPs was added for every 100 mg collagen such that the final collagen matrix contained ~13.6 wt% or ~1.0 vol% Au NPs.

The mixture of collagen fibrils and MSA-Au NPs was collected and concentrated by centrifugation at ~11,000*g* for 30 min, and the supernatant was decanted. Paraffin microspheres, 300-425 μm in diameter, were prepared using methods previously described in detail [24]. 585 mg of paraffin microspheres was added to the concentrated collagen slurry and mixed thoroughly. The resulting slurry containing concentrated collagen fibrils, MSA-Au NPs, and paraffin microspheres was compression molded at 1 MPa for 3 min to form cylindrical pellets 6 mm in diameter and ~6 mm in height. As-molded pellets were sectioned to 3 mm in height and a biopsy punch was used to remove cylindrical pellets 3 mm in diameter. These pellets were washed four times with 100% hexane for 12 h per wash and twice with 100% ethanol for 8 h per wash to remove the paraffin microspheres, resulting in porous scaffolds. Scaffolds were subsequently crosslinked for 12 h under gentle stirring in an 80% solution of ethanol in DI water containing 20 mM 1-ethyl-3-(3-dimethylaminopropyl)carbodiimide (EDC, Sigma-Aldrich) and 8 mM *n*-hydroxysuccinimide (NHS, Sigma-Aldrich) [24,49]. The resulting crosslinked scaffolds were rinsed with 100% ethanol and stored in either 100% ethanol or sterile 1X phosphate buffered saline (PBS), depending on subsequent use described below, until further use.

Characterization of as-prepared scaffolds

Micro-CT. The microarchitecture of collagen scaffolds conjugated with 80 mM Au NPs was characterized by micro-CT (Skyscan 1172, Bruker) in either air or DI water. As-prepared scaffolds were fixed with 2% glutaraldehyde in 0.1 M sodium cacodylate buffer. Dried scaffolds were dehydrated in a graded series of ethanol concentrations (50-100%) over 2 days before critical point drying (EM CPD300, Leica) in 100% ethanol. Micro-CT images were acquired at 34 kVp and 210 µA with no beam filtration, 1200 projections at 1100 ms integration time, and a 2.35 µm isotropic voxel size. Wet scaffolds were stained with 1% osmium tetroxide in distilled water for 60 min before and after treating with 0.5% thiocarbohydrazide in DI water for 30 min [50]. Micro-CT images were acquired at 44 kVp voltage and 222 µA current with 0.5 mm aluminum beam filtration, 1200 projections at 950 ms integration time, and a 3.42 µm isotropic voxel size.

Three-dimensional (3D) images were reconstructed using the Feldkamp algorithm [51] (NRrecon v1.7.3.1, Bruker). The total scaffold porosity (vol%) was measured after segmenting images with a global threshold determined from the image intensity histogram and removing objects comprising less than 75 pixels in any image slice with a despeckle filter (CTan v1.16.4.1, Bruker). The pore interconnectivity, or percent open porosity, was measured as a percent of the total scaffold porosity. The pore size distribution was measured from 2D image slices of representative dry (n = 1719 pores) and wet scaffolds (n = 1296 pores) (ImageJ v1.49, National Institutes of Health). The pore size distribution was also measured from a 3D reconstruction of a representative dry scaffold (n = 502 pores) after applying a median filter, segmenting porosity, applying an erosion filter (10 pixel ball kernel) and watershed separation (marker extent = 4), and assuming spherical pores (Avizo v9.0, FEI).

The effect of the Au NP concentration on the X-ray attenuation of collagen scaffolds was measured by micro-CT (µCT-80, Scanco Medical AG) at 70 kVp and 144 µA, with 0.5 mm aluminum beam filtration, 720 projections at 800 ms integration time, and a 10 µm isotropic voxel size. As-prepared collagen scaffolds were dried and imaged in air within Eppendorf tubes. A cylindrical volume of interest (VOI), ~3 mm in diameter and height (~21 mm^3), was used for analysis of the entire scaffold volume including the collagen matrix and porosity. The mean linear attenuation coefficient (cm^{-1}) measured for each scaffold VOI was converted to Hounsfield units (HU) using an internal sample calibration for air (-1000 HU) and water (0 HU) in the same image acquisition. The measured X-ray attenuation of collagen scaffolds with varying concentration of Au NPs was reported as the mean (± standard deviation) of four replicates per group and modeled using linear least squares regression (JMP 13, SAS Institute, Inc.). The mean X-ray attenuation of scaffolds was compared to PBS, as a surrogate for soft tissue, using one-sample Student's *t*-tests with a hypothesized mean of 58 HU, which corresponded to the measured X-ray attenuation of PBS. The level of significance for all tests was set at $p < 0.05$.

Electron microscopy and tomography. The nanostructure of collagen scaffolds conjugated with 80 mM Au NPs was characterized by transmission electron microscopy (TEM) and electron tomography. As-prepared scaffolds were fixed with 2% glutaraldehyde in 0.1 M sodium cacodylate buffer, dehydrated in a graded series of ethanol concentrations (50-100%) over 2 days, embedded in epoxy (EMbed 812, Electron Microscopy Sciences), and sectioned to 80 nm thickness using an ultramicrotome (Ultracut UCT, Leica). Sections were placed on copper grids and stained with a saturated uranyl acetate solution in 50% ethanol for 5 min followed by Reynolds' lead citrate stain [52] for 3 min. Sections were imaged by TEM (JEM-1200EX, JEOL Ltd.) at 80 kV accelerating voltage.

Electron tomography was performed using a scanning transmission electron microscope (STEM, Titan 80-300, FEI) operating at 300 kV accelerating voltage with a convergence angle of 6.24 mrad and a high angle annular dark field (HAADF) detector. A tilt series of image projections was acquired every 2° from -65° to +75°, aligned via cross-correlation, and reconstructed using a simultaneous iterative reconstruction method (SIRT) with 20 iterations (Inspect 3D, v4.0, FEI). The dispersion and agglomeration of Au NPs within the collagen matrix was measured and visualized by color coding the volume of individual and agglomerated NPs within 3D images (Avizo v9.2, FEI).

In vitro enzymatic degradation of collagen scaffolds

Collagen scaffolds conjugated with 80 mM Au NPs were incubated at 37ºC in media (Dulbecco's PBS with $MgCl_2$ and $CaCl_2$, Sigma-Aldrich) containing 0, 0.3, or 0.5 mg/ml bacterial (*Clostridium histolyticum*) collagenase (Collagenase B, >0.15 Wünsch U/mg, Roche Diagnostics GmbH) as an *in vitro* model of enzymatic degradation. Scaffolds were placed in individual 1.5 mL Eppendorf tubes containing the incubation media. For each longitudinal time point, the media was separated from the scaffold and/or scaffold fragments by centrifugation at 500*g* for 1 min and collected for analysis by inductively-coupled plasma optical emission spectroscopy (ICP-OES), as described below. The wet weight of the remaining scaffold was measured, fresh media lacking collagenase was added to the tube, the scaffold was imaged by micro-CT as described below, and then additional fresh media containing collagenase was added to the tube for continued degradation. Note that scaffolds from all groups were first incubated in media not containing collagenase for 24 h to establish the initial (day 0) time point. Longitudinal measurements were subsequently taken every 24 h until the scaffold was fully degraded. Scaffold degradation was measured gravimetrically by the difference in scaffold weight relative to the initial scaffold weight on day 0, such that the measurement bounds were 0 to 100 wt%.

Micro-CT. The degradation kinetics of collagen scaffolds was measured by micro-CT (μCT-80, Scanco Medical AG) at 70 kVp and 144 μA, with 0.5 mm aluminum beam filtration, 125 projections at 800 ms integration time, and a 100 μm isotropic voxel size chosen to replicate *in vivo* imaging methods. Scaffolds were imaged while submerged in 50 μL PBS within Eppendorf tubes. Noise in grayscale images was reduced using a Gaussian filter (sigma = 0.8, support = 1). The overall VOI for analysis included the entire volume of the media containing the scaffold and/or scaffold fragments (~90-140 mm^3). The scaffold volume was segmented from media using a fixed global threshold of 110, which corresponded to a linear attenuation of 0.88 cm^{-1} or ~830 HU. Scaffold degradation was measured by the difference in segmented scaffold volume relative to the initial scaffold volume on day 0, such that the measurement bounds were 0 to 100 vol%. Scaffold degradation was also measured by the mean X-ray attenuation (HU) within the overall VOI to replicate possible *in vivo* imaging methods. The two measurement methods were correlated by linear least squares regression (JMP 13).

ICP-OES. The Au concentration in as-prepared solutions of Au NPs and in supernatant media during *in vitro* enzymatic degradation of collagen scaffolds was measured using ICP-OES (Optima 7000, Perkin Elmer) after digesting samples in 3% aqua regia (3 parts HCl to 1 part HNO_3). Calibration curves were created by diluting certified standard Au solutions (Assurance Grade, SPEX CertiPrep). Scaffold degradation was measured by the cumulative release of Au into the media relative to the total amount of Au in the scaffold, such that the measurement bounds were 0 to 100 wt% Au.

Degradation kinetics. The percent scaffold degradation measured by micro-CT, ICP-OES, and gravimetric analysis at each longitudinal time point was reported as the mean (± standard deviation) of five replicates. Scaffold degradation kinetics were modeled by non-linear least squares regression (JMP 13) using a three-parameter logistic equation,

$$y = \frac{c}{(1 + \exp(-a \cdot (t - b))}$$

where y is the scaffold degradation (%), a is the growth parameter (days^{-1}), b is the inflection parameter (days), and c is the asymptote parameter (%), and t is time (days). The scaffold degradation half-life (t_{50}) and 95% confidence interval were also determined from the model. Differences in the degradation kinetics between groups (collagenase concentration and measurement method) were examined by multivariate analysis of variance using a generalized linear model (GLM) with a binomial distribution and logit link function, while accounting for sample replicates as a factor in the model (JMP 13). The level of significance for all tests was set at $p < 0.05$.

Acknowledgments

This research was partially supported by the National Science Foundation (DMR-1309587), International Precious Metals Institute, Kelly Cares Foundation, St. Joseph Health System, and the Walter Cancer Research Institute. The authors also acknowledge the Center for Environmental Science and Technology at the University of Notre Dame for the use of ICP-OES.

References

1. M. Geiger, R.H. Li and W. Friess, Collagen sponges for bone regeneration with rhBMP-2, *Adv. Drug Deliv. Rev.*, 2003, 55, 1613–29.
2. M. Sokolsky-Papkov, K. Agashi, A. Olaya, K. Shakesheff and A.J. Domb, Polymer carriers for drug delivery in tissue engineering, *Adv. Drug Deliv. Rev.*, 2007, 59, 187–206.
3. H.J. Chung and T.G. Park, Surface engineered and drug releasing pre-fabricated scaffolds for tissue engineering, *Adv. Drug Deliv. Rev.*, 2007, 59, 249–62.
4. B. Dhandayuthapani, Y. Yoshida, T. Maekawa and D.S. Kumar, Polymeric scaffolds in tissue engineering application: A review, *Int. J. Polym. Sci.*, 2011, 290602.
5. T. Okada, T. Hayashi and Y. Ikada, Degradation of collagen suture *in vitro* and *in vivo*, *Biomaterials*, 1992, 13, 448–54.
6. L.H.H. Olde Damink, P.J. Dijkstra, M.J.A. Van Luyn, P.B. Van Wachem, P. Nieuwenhuis and J. Feijen, Changes in the mechanical properties of dermal sheep collagen during *in vitro* degradation, *J. Biomed. Mater. Res.*, 1995, 29, 139–47.
7. L. Wu and J. Ding, *In vitro* degradation of three-dimensional porous poly(D,L-lactide-*co*-glycolide) scaffolds for tissue engineering, *Biomaterials*, 2004, 25, 5821–30.
8. C.X.F. Lam, D.W. Hutmacher, J-T. Schantz, M.A. Woodruff and S.H. Teoh, Evaluation of polycaprolactone scaffold degradation for 6 months *in vitro* and *in vivo*, *J. Biomed. Mater. Res.*, 2009, 90A, 906–19.
9. L. Lu, S.J. Peter, M.D. Lyman, H-L. Lai, S.M. Leite, J.A. Tamada, S. Uyama, J.P. Vacanti, R. Langer and A.G. Mikos, *In vitro* and *in vivo* degradation of porous poly(D,L-lactide-*co*-glycolide) foams, *Biomaterials*, 2000, 21, 137–45.
10. L. Ma, C. Gao, Z. Mao, J. Zhou, J. Shen, X. Hu and C. Han, Collagen/chitosan porous scaffolds

with improved biostability for skin tissue engineering, *Biomaterials*, 2003, 24, 4833–41.

11. N. Artzi, N. Oliva, C. Puron, S. Shitreet, S. Artzi, A.B. Ramos, A. Groothuis, G. Sahagian and E.R. Edelman, *In vivo* and *in vitro* tracking of erosion in biodegradable materials using non-invasive fluorescence imaging, *Nat. Mater.*, 2011, 10, 704–9.
12. S.H. Kim, J.H. Lee, H. Hyun, Y. Ashitate, G.L. Park, K. Robichaud, E. Lunsford, S.J. Lee, G. Khang and H.S. Choi, Near-infrared fluorescence imaging for noninvasive trafficking of scaffold degradation, *Sci. Rep.*, 2013, 3, 1198.
13. W. Wang, J. Liu, C. Li, J. Zhang, J. Liu, A. Dong and D. Kong, Real-time and non-invasive fluorescence tracking of *in vivo* degradation of the thermosensitive PEGylated polyester hydrogel, *J. Mater. Chem. B*, 2014, 2, 4185–92.
14. L.S. Karfield-Sulzer, E.A. Waters, E.K. Kohlmeir, H. Kissler, X. Zhang, D.B. Kaufman, A.E. Barron and T.J. Meade, Protein polymer MRI contrast agents: Longitudinal analysis of biomaterials *in vivo*, *Magn. Reson. Med.*, 2011, 65, 220–8.
15. Y. Sun, P. Geutjes, E. Oosterwijk and A. Heerschap, *In vivo* magnetic resonance imaging of type I collagen in rat: improving visualization of bladder and subcutaneous implants, *Tissue Eng. Part C Methods*, 2014, 20, 964–71.
16. A.A. Appel, M.A. Anastasio, J.C. Larson and E.M. Brey, Imaging challenges in biomaterials and tissue engineering, *Biomaterials*, 2013, 34, 6615–30.
17. K. Kim, C.G. Jeong and S.J. Hollister, Non-invasive monitoring of tissue scaffold degradation using ultrasound elasticity imaging, *Acta Biomater.*, 2008, 4, 783–90.
18. D.W. Park, S-H. Ye, H.B. Jiang, D. Dutta, K. Nonaka, W.R. Wagner and K. Kim, *In vivo* monitoring of structural and mechanical changes of scaffolds by multi-modality imaging, Biomaterials, 2014, 35, 7851–9.

19. K. Kim and W.R. Wagner, Non-invasive and non-destructive characterization of tissue engineered constructs using ultrasound imaging technologies: A review, *Ann. Biomed. Eng.*, 2016, 44, 621–35.
20. E. Behravesh, M.D. Timmer, J.J. Lemoine, M.A. Liebschner and A.G. Mikos, Evaluation of the *in vitro* degradation of microporous hydrogels using gravimetry, confined compression testing, micro-computed tomography, *Biomacromolecules*, 2002, 3, 1263–70.
21. E.L. Hedberg, C.K. Shih, J.J. Lemoine, M.D. Timmer, M.A.K. Liebschner, J.A. Jansen and A.G. Mikos, *In vitro* degradation of porous poly(propylene fumarate)/poly(DL-lactic-*co*-glycolic acid) composite scaffolds, *Biomaterials*, 2005, 26, 3215–25.
22. S.M. Forton, M.T. Latourette, M. Parys, M. Kiupel, D. Shahriari, J.S. Sakamoto and E.M. Shapiro, *In vivo* microcomputed tomography of nanocrystal-doped tissue engineered scaffolds, *ACS Biomater. Sci. Eng.*, 2016, 2, 508–16.
23. L.E. Cole, R.D. Ross, J.M.R. Tilley, T. Vargo-Gogola and R.K. Roeder, Gold nanoparticles as contrast agents in X-ray imaging and computed tomography, *Nanomedicine*, 2015, 10, 321–41.
24. R.J. Kane, H.E. Weiss-Bilka, M.J. Meagher, Y. Liu, J.A. Gargac, G.L. Niebur, D.R. Wagner and R.K. Roeder, Hydroxyapatite reinforced collagen scaffolds with improved architecture and mechanical properties, *Acta Biomater.*, 2015, 17, 16–25.
25. M.J. Meagher, H.E. Weiss-Bilka, M.E. Best, J.D. Boerckel, D.R. Wagner and R.K. Roeder, Acellular hydroxyapatite-collagen scaffolds support angiogenesis and osteogenic gene expression in an ectopic murine model: Effects of hydroxyapatite volume fraction, *J. Biomed. Mater. Res.*, 2016, 104A, 2178–88.
26. P.B. Malafaya, G.A. Silva and R.L. Reis, Natural–origin polymers as carriers and scaffolds for

biomolecules and cell delivery in tissue engineering applications, *Adv. Drug Deliv. Rev.*, 2007, 59, 207–33.

27. E. Sachlos, N. Reis, C. Ainsley, B. Derby and J.T. Czernuszka, Novel collagen scaffolds with predefined internal morphology made by solid freeform fabrication, *Biomaterials*, 2003, 24 1487–97.

28. W-Y. Yeong, C-K. Chua, K-F. Leong, M. Chandrasekaran and M-W. Lee, Comparison of drying methods in the fabrication of collagen scaffold via indirect rapid prototyping, *J. Biomed. Mater. Res.*, 2007, 82B, 260–6.

29. Y. Nakashima and T. Nakano, Optimizing contrast agents with respect to reducing beam hardening in nonmedical X-ray computed tomography experiments, *J. X-Ray Sci. Technol.*, 2014, 22, 91–103.

30. P.D. Nallathamby, J. Hopf, L.E. Irimata, T.L. McGinnity and R.K. Roeder, Preparation of fluorescent Au–SiO_2 core–shell nanoparticles and nanorods with tunable silica shell thickness and surface modification for immunotargeting, *J. Mater. Chem. B*, 2016, 4, 5418–28.

31. P.C. Naha, A.A. Zaki, E. Hecht, M. Chorny, P. Chhour, E. Blankemeyer, D.M. Yates, W.R.T. Witschey, H.I. Litt, A. Tsourkas and D.P. Cormode, Dextran coated bismuth–iron oxide nanohybrid contrast agents for computed tomography and magnetic resonance imaging, *J. Mater. Chem. B*, 2014, 2, 8239–48.

32. T.L. McGinnity, O. Dominguez, T.E. Curtis, P.D. Nallathamby, A.J. Hoffman and R.K. Roeder, Hafnia (HfO_2) nanoparticles as an X-ray contrast agent and mid-infrared biosensor, *Nanoscale*, 2016, 8, 13627–37.

33. B.M. Yeh, P.F. FitzGerald, P.M. Edic, J.W. Lambert, R.E. Colborn, M.E. Marino, P.M. Evans, J.C. Roberts, Z.J. Wang, M.J. Wong and P.J. Bonitatibus, Opportunities for new CT contrast

agents to maximize the diagnostic potential of emerging spectral CT technologies, *Adv. Drug Delivery Rev.*, 2017, 113, 201–22.

34. S.A. Grant, C.S. Spradling, D.N. Grant, D.B. Fox, L. Jimenez, D.A. Grant and R.J. Rone, Assessment of the biocompatibility and stability of a gold nanoparticle collagen bioscaffold, *J. Biomed. Mater. Res.*, 2014, 102A, 332–9.
35. A.M. Ostdiek, J.R. Ivey, D.A. Grant, J. Gopaldas and S.A. Grant, An *in vivo* study of a gold nanocomposite biomaterial for vascular repair, *Biomaterials*, 2015, 65, 175–183.
36. L.E. Cole, T.L. McGinnity, L.E. Irimata, T. Vargo-Gogola and R.K. Roeder, Effects of bisphosphonate ligands and PEGylation on targeted delivery of gold nanoparticles for contrast-enhanced radiographic detection of breast microcalcifications, *Acta Biomater.*, 2018, 82, 122–32.
37. H.E. Weiss-Bilka, M.E. McGann, M.J. Meagher, R.K. Roeder and D.R. Wagner, Ectopic models for endochondral ossification: comparing pellet and alginate bead culture methods, *J. Tissue Eng. Regen. Med.*, 2016, 12, e541–9.
38. C.M. Murphy, A. Schindeler, J.P. Gleeson, N. Yu, L.C. Cantril, K. Mikulec, L. Peacock, F.J. O'Brien and D.G. Little, A collagen–hydroxyapatite scaffold allows for binding and co-delivery of recombinant bone morphogenetic proteins and bisphosphonates, *Acta Biomater.*, 2014, 10, 2250–8.
39. R.E. Geuze, L.F.H. Theyse, D.H.R. Kempen, H.A.W. Hazewinkel, H.Y.A. Kraak, F.C. Öner, W.J.A. Dhert and J. Alblas, A Differential effect of bone morphogenetic protein-2 and vascular endothelial growth factor release timing on osteogenesis at ectopic and orthotopic sites in a large-animal model, *Tissue Eng.*, 2012, 18, 2052–62.
40. J.D. Boerckel, Y.M. Kolambker, K.M. Dupont, B.A. Uhrig, E.A. Phelps, H.Y. Stevens, A.J.

Garcia and R.E. Guldberg, Effects of protein dose and delivery system on BMP-mediated bone regeneration, *Biomaterials*, 2011, 22, 5241–51.

41. F.G. Lyons, A.A. Al-Munajjed, S.M. Kieran, M.E. Toner, C.M. Murphy, G.P. Duffy and F.J. O'Brien, The healing of bony defects by cell-free collagen-based scaffolds compared to stem cell-seeded tissue engineered constructs, *Biomaterials*, 2010, 31, 9232–43.
42. T.E. Curtis, R.K. Roeder, Quantification of mixed contrast and tissue compositions using photon-counting spectral computed tomography, *J. Med. Imaging*, in press.
43. A. Yahyouche, X. Zhidao, J.T. Czernuszka and A.J. Clover, Macrophage-mediated degradation of crosslinked collagen scaffolds, *Acta Biomater*., 2011, 7, 278-86.
44. O. Jeon, K.H. Bouhadir, J.M. Mansour and E. Alsberg, Photocrosslinked alginate hydrogels with tunable biodegradation rates and mechanical properties, *Biomaterials*, 2009, 30, 2724–34.
45. J.D. Boerckel, D.E. Mason, A.M. McDermott and E. Alsberg, Microcomputed tomography: approaches and applications in bioengineering, *Stem Cell Res. Ther*., 2014, 5, 144.
46. R.D. Ross and R.K. Roeder, Binding affinity of surface functionalized gold nanoparticles to hydroxyapatite, *J. Biomed. Mater. Res*., 2011, 99A, 58–66.
47. R.D. Ross, L.E. Cole, J.M.R. Tilley and R.K. Roeder, Effects of functionalized gold nanoparticle size on X-ray attenuation and substrate binding affinity, *Chem. Mater*., 2014, 26 1187–94.
48. J. Black and R.U. Mattson, Relationship between porosity and mineralization in the Haversian osteon, *Calcif. Tissue Int*., 1982, 34, 332–6.
49. L.H. Olde Damink, P.J. Dijkstra, M.J. van Luyn, P.B. van Wachem, P. Nieuwenhuis and J. Feijen, Cross-linking of dermal sheep collagen using a water-soluble carbodiimide,

Biomaterials, 1996, 17, 765–73.

50. N. Reznikov, R. Almany-Magal, R. Shahar and S. Wiener, Three-dimensional imaging of collagen fibril organization in rat circumferential lamellar bone using a dual beam electron microscope reveals ordered and disordered sub-lamellar structures, *Bone*, 2013, 52, 676–83.
51. L.A. Feldkamp, L.C. Davis and J.W. Kress, Practical cone-beam algorithm, *J. Opt. Soc. Am. A*, 1984, 1, 612–9.
52. E.S. Reynolds, The use of lead citrate at high pH as an electron-opaque stain in electron microscopy, *J. Cell Biol.*, 1963, 17, 208–12.

Tables

Table 1: Non-linear least squares regression of the measured collagen scaffold degradation kinetics (Fig. 5) using a three-parameter logistic model (Eq. 1) where *a* is the growth parameter (days^{-1}), *b* is the inflection parameter (days), *c* is the asymptote parameter (%), R^2 is the correlation coefficient, and t_{50} is the scaffold degradation half-life. The standard error of fitting parameters and the 95% confidence interval of t_{50} are shown in parentheses.

Collagenase Concentration (mg/ml)	Method	*a* (days^{-1})	*b* (days)	*c* (%)	R^2	t_{50} (days)
0.3	Micro-CT	1.10 (0.09)	3.19 (0.09)	92.41 (1.73)	0.97	3.34 (3.19-3.50)
	ICP-OES	0.89 (0.08)	3.60 (0.12)	95.37 (2.39)	0.96	3.71 (3.52-3.90)
	Gravimetric	2.55 (1.18)	2.09 (0.17)	81.63 (3.73)	0.73	2.27 (1.89-2.64)
0.5	Micro-CT	2.06 (0.18)	1.21 (0.05)	98.25 (1.01)	0.97	1.22 (1.14-1.31)
	ICP-OES	1.56 (0.10)	1.47 (0.05)	96.86 (0.88)	0.98	1.50 (1.42-1.59)
	Gravimetric	7.29 (164)	0.96 (0.93)	88.46 (5.40)	0.42	1.00 (0.71-1.28)

Figure Captions

Fig. 1 Schematic diagram showing conjugation of MSA functionalized Au NPs to type I collagen. (a) Thiol groups on MSA were covalently linked to Au NP surfaces and (b) carboxyl groups on MSA were covalently linked to amine groups on collagen molecules using EDC/NHS chemistry, such that Au NPs were released only upon enzymatic degradation of collagen scaffolds.

Fig. 2 Hierarchical structure of collagen scaffolds covalently conjugated with 80 mM Au NPs. (a) Representative grayscale micro-CT image slice showing the collagen scaffold microarchitecture in a transverse cross-section. Representative TEM micrographs of the collagen matrix showing (b) collagen fibrils, which are oriented horizontally, conjugated with Au NPs, which are spatially associated with collagen fibrils, and (c) the conjugated Au NPs at higher magnification.

Fig. 3 Quantitative 3D characterization of the microarchitecture and nanostructure of a representative collagen scaffold covalently conjugated with 80 mM Au NPs. 3D micro-CT reconstructions showing (a) the scaffold microarchitecture, including orthogonal grayscale image slices, and (b) the segmented pore structure, including the distribution of pore volumes. (c) 3D electron tomography reconstruction of a thin section from the collagen matrix showing segmented Au NPs, including the distribution of NP aggregates, (d) which was also plotted as a histogram.

Fig. 4 (a) Representative grayscale micro-CT image slices of collagen scaffolds containing 0, 20, 40, 60, and 80 mM Au NPs. Scale bar = 1 mm. (b) The measured X-ray attenuation of scaffolds increased linearly with increased Au NP concentration ($p < 0.0001$) and was strongly correlated ($R^2 = 0.95$). Scaffolds containing at least 60 mM Au NPs exhibited significantly greater X-ray attenuation than PBS ($p < 0.005$, *t*-test vs. 58 HU), which was chosen to be representative of soft tissue. Note that scaffolds were imaged in air and the VOI for (b) included the entire scaffold volume inclusive of porosity (air). Thus, scaffolds without Au NPs exhibited the attenuation of air, approximately -1000 HU.

Fig. 5 Collagen scaffold degradation kinetics in media containing 0, 0.3, and 0.5 mg/ml collagenase was measured longitudinally *in vitro* by (a) the segmented scaffold volume using contrast-enhanced micro-CT, including representative grayscale micro-CT image slices for selected time points (scale bar = 1 mm), (b) the cumulative release of Au NPs into the media using ICP-OES, and (c) the scaffold mass using gravimetric analysis. Error bars show one standard deviation of the mean (n = 5/group/time point). Error bars not shown lie within the data point. The scaffold degradation kinetics increased with an increased concentration of collagenase in the media ($p < 0.0001$, GLM), as expected; scaffolds exhibited no degradation and minimal (~5 %) release of Au NPs in the absence of collagenase. The scaffold degradation kinetics were modeled by non-linear least squares regression using a three-parameter logistic equation (Table 1).

Fig. 6 The mean X-ray attenuation (HU) measured by micro-CT within a fixed VOI, including the entire volume of the media containing the scaffold and/or scaffold fragments, decreased linearly and was strongly correlated ($R^2 = 0.84$) with the cumulative degradation determined from the segmented scaffold volume in micro-CT. Note that the x-axis corresponds to all longitudinal measurements in Fig. 5a for enzymatic scaffold degradation in media containing 0.3 and 0.5 mg/ml collagenase. Measurements for media containing 0 mg/ml collagenase were omitted for clarity as these scaffolds did not exhibit degradation and all data points were thus clustered at approximately 0 vol% cumulative degradation and 100 HU.

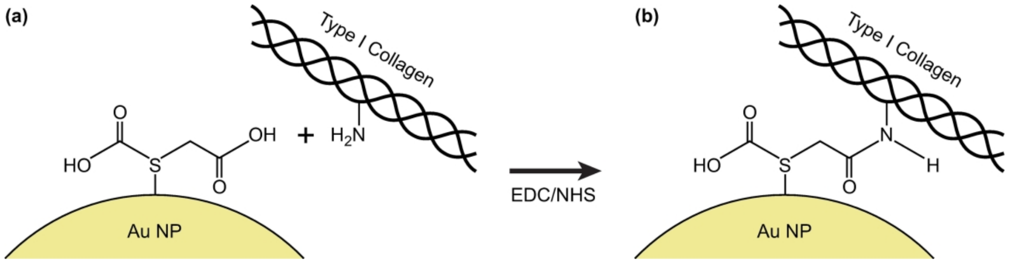

Fig. 1 Schematic diagram showing conjugation of MSA functionalized Au NPs to type I collagen. (a) Thiol groups on MSA were covalently linked to Au NP surfaces and (b) carboxyl groups on MSA were covalently linked to amine groups on collagen molecules using EDC/NHS chemistry, such that Au NPs were released only upon enzymatic degradation of collagen scaffolds.

223x57mm (300 x 300 DPI)

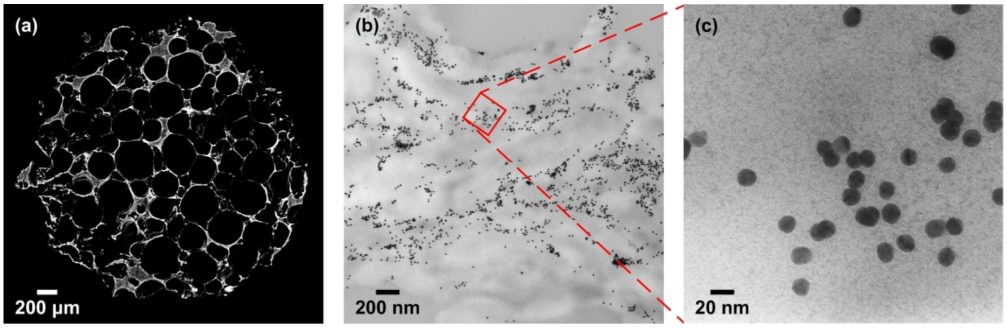

Fig. 2 Hierarchical structure of collagen scaffolds covalently conjugated with 80 mM Au NPs. (a) Representative grayscale micro-CT image slice showing the collagen scaffold microarchitecture in a transverse cross-section. Representative TEM micrographs of the collagen matrix showing (b) collagen fibrils, which are oriented horizontally, conjugated with Au NPs, which are spatially associated with collagen fibrils, and (c) the conjugated Au NPs at higher magnification.

223x71mm (300 x 300 DPI)

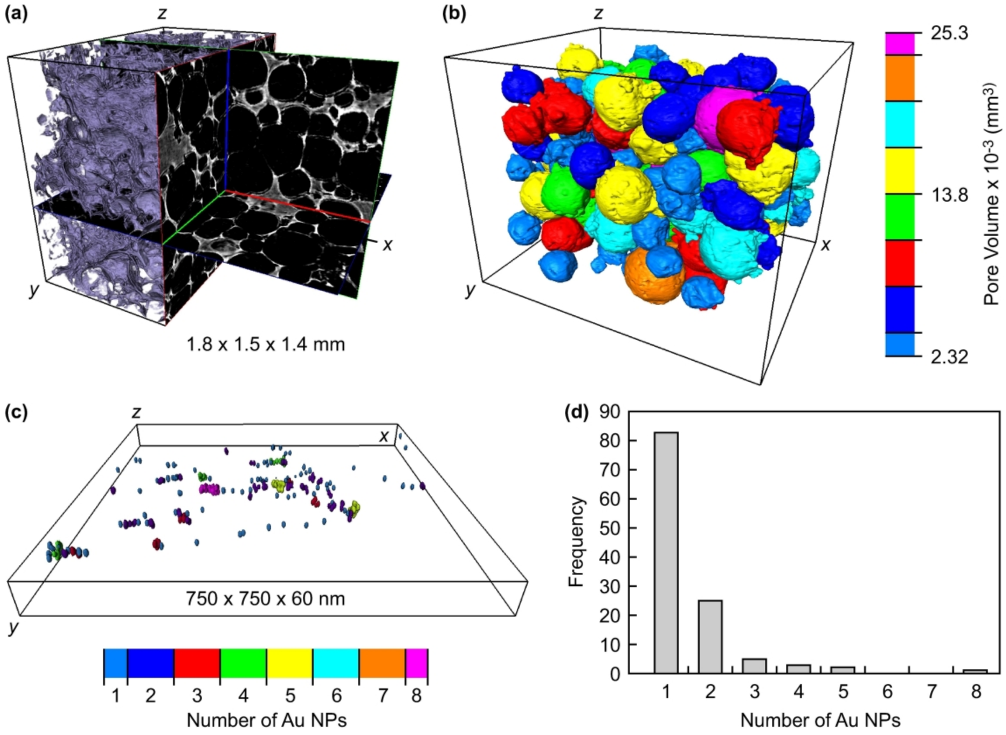

Fig. 3 Quantitative 3D characterization of the microarchitecture and nanostructure of a representative collagen scaffold covalently conjugated with 80 mM Au NPs. 3D micro-CT reconstructions showing (a) the scaffold microarchitecture, including orthogonal grayscale image slices, and (b) the segmented pore structure, including the distribution of pore volumes. (c) 3D electron tomography reconstruction of a thin section from the collagen matrix showing segmented Au NPs, including the distribution of NP aggregates, (d) which was also plotted as a histogram.

218x159mm (300 x 300 DPI)

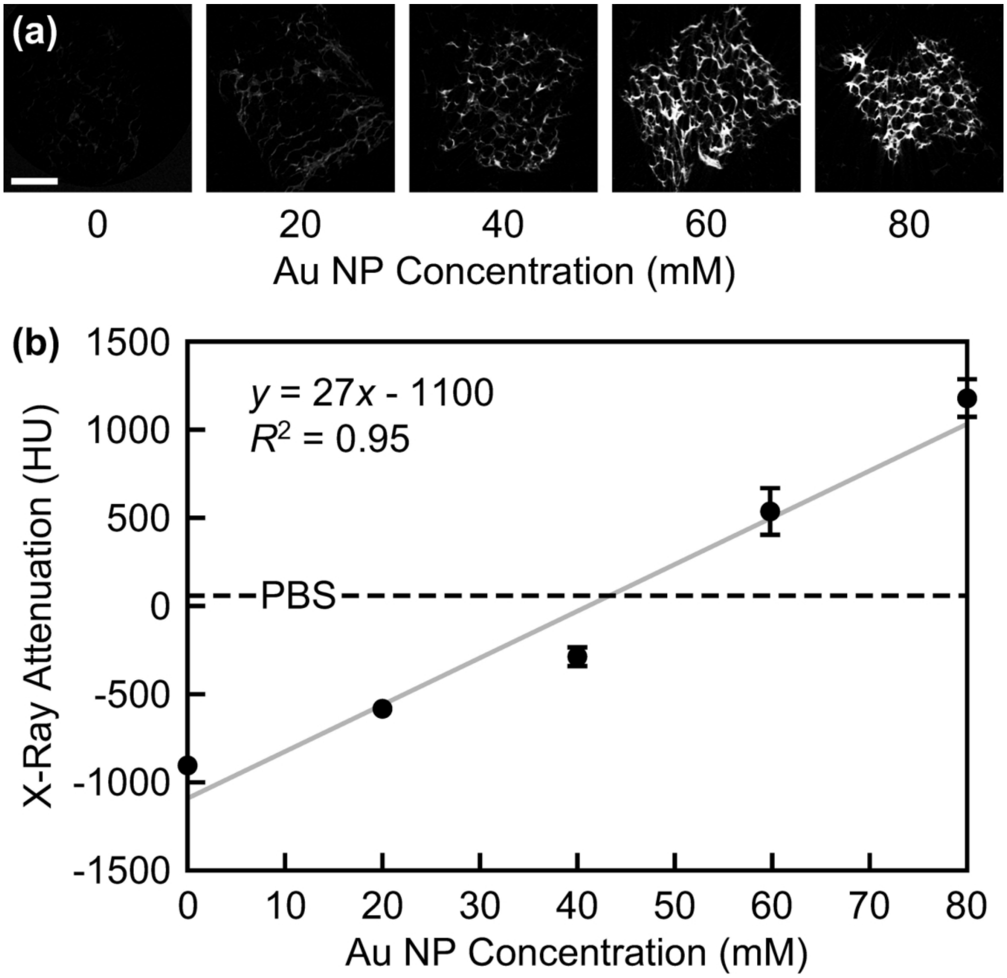

Fig. 4 (a) Representative grayscale micro-CT image slices of collagen scaffolds containing 0, 20, 40, 60, and 80 mM Au NPs. Scale bar = 1 mm. (b) The measured X-ray attenuation of scaffolds increased linearly with increased Au NP concentration ($p < 0.0001$) and was strongly correlated ($R^2 = 0.95$). Scaffolds containing at least 60 mM Au NPs exhibited significantly greater X-ray attenuation than PBS ($p < 0.005$, *t*-test vs. 58 HU), which was chosen to be representative of soft tissue. Note that scaffolds were imaged in air and the VOI for (b) included the entire scaffold volume inclusive of porosity (air). Thus, scaffolds without Au NPs exhibited the attenuation of air, approximately -1000 HU.

164x160mm (300 x 300 DPI)

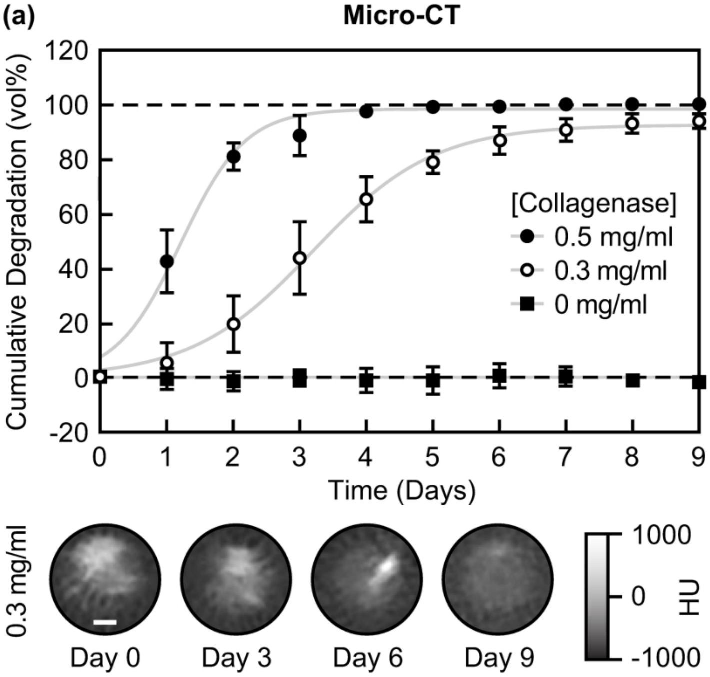

Fig. 5 Collagen scaffold degradation kinetics in media containing 0, 0.3, and 0.5 mg/ml collagenase was measured longitudinally in vitro by (a) the segmented scaffold volume using contrast-enhanced micro-CT, including representative grayscale micro-CT image slices for selected time points (scale bar = 1 mm), (b) the cumulative release of Au NPs into the media using ICP-OES, and (c) the scaffold mass using gravimetric analysis. Error bars show one standard deviation of the mean (*n* = 5/group/time point). Error bars not shown lie within the data point. The scaffold degradation kinetics increased with an increased concentration of collagenase in the media ($p < 0.0001$, GLM), as expected; scaffolds exhibited no degradation and minimal (~5 %) release of Au NPs in the absence of collagenase. The scaffold degradation kinetics were modeled by non-linear least squares regression using a three-parameter logistic equation (Table 1).

215x279mm (300 x 300 DPI)

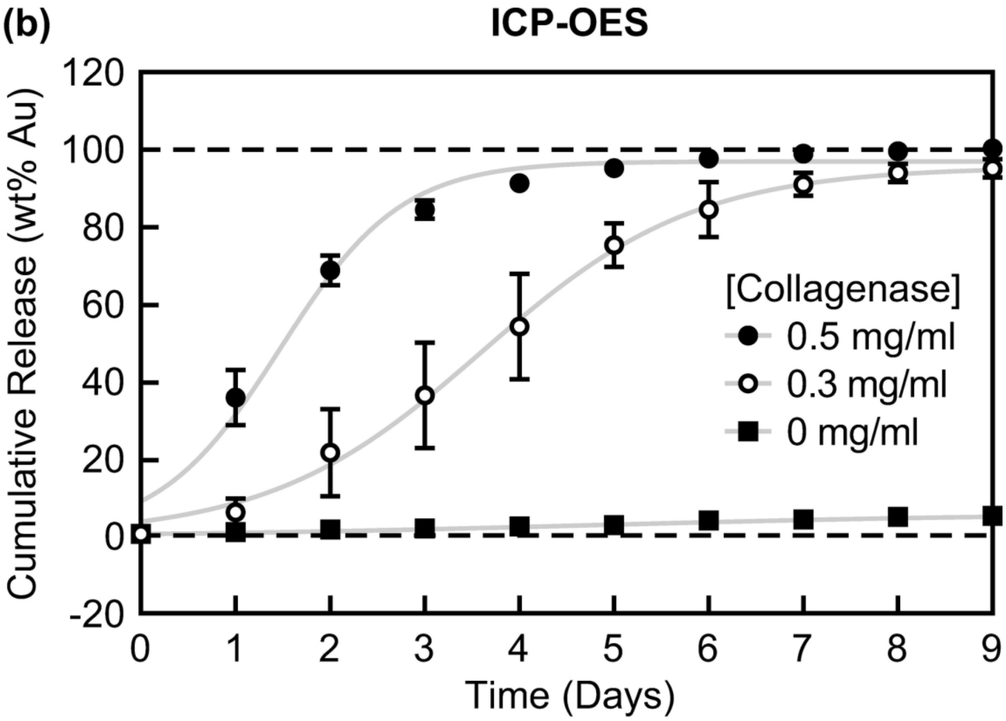

Fig. 5 Collagen scaffold degradation kinetics in media containing 0, 0.3, and 0.5 mg/ml collagenase was measured longitudinally in vitro by (a) the segmented scaffold volume using contrast-enhanced micro-CT, including representative grayscale micro-CT image slices for selected time points (scale bar = 1 mm), (b) the cumulative release of Au NPs into the media using ICP-OES, and (c) the scaffold mass using gravimetric analysis. Error bars show one standard deviation of the mean (*n* = 5/group/time point). Error bars not shown lie within the data point. The scaffold degradation kinetics increased with an increased concentration of collagenase in the media ($p < 0.0001$, GLM), as expected; scaffolds exhibited no degradation and minimal (~5 %) release of Au NPs in the absence of collagenase. The scaffold degradation kinetics were modeled by non-linear least squares regression using a three-parameter logistic equation (Table 1).

164x118mm (300 x 300 DPI)

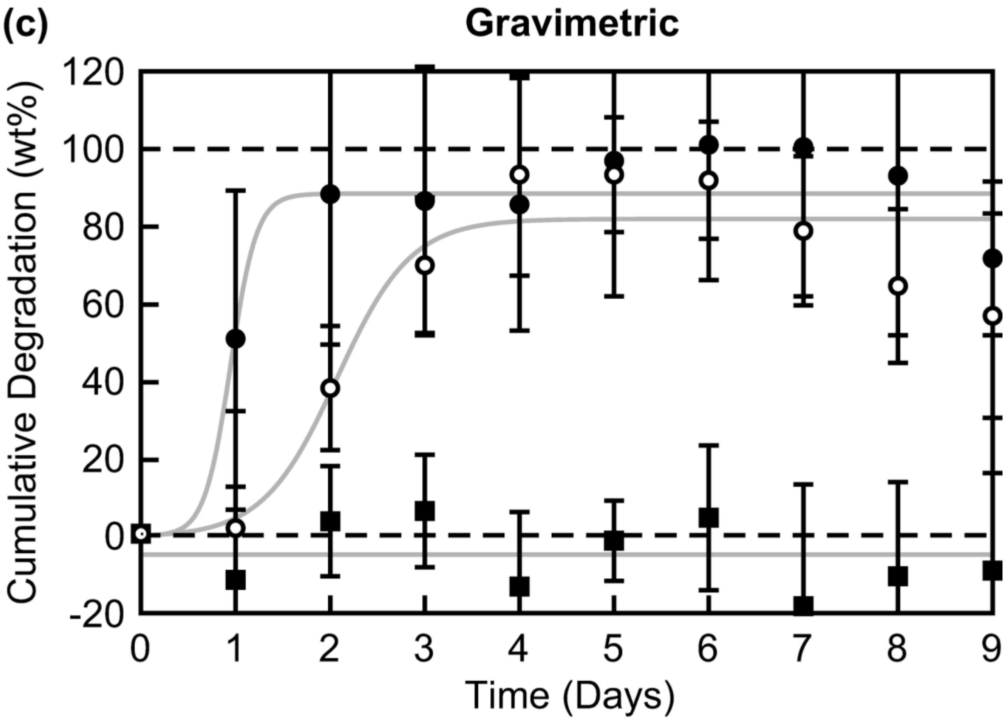

Fig. 5 Collagen scaffold degradation kinetics in media containing 0, 0.3, and 0.5 mg/ml collagenase was measured longitudinally in vitro by (a) the segmented scaffold volume using contrast-enhanced micro-CT, including representative grayscale micro-CT image slices for selected time points (scale bar = 1 mm), (b) the cumulative release of Au NPs into the media using ICP-OES, and (c) the scaffold mass using gravimetric analysis. Error bars show one standard deviation of the mean (*n* = 5/group/time point). Error bars not shown lie within the data point. The scaffold degradation kinetics increased with an increased concentration of collagenase in the media ($p < 0.0001$, GLM), as expected; scaffolds exhibited no degradation and minimal (~5 %) release of Au NPs in the absence of collagenase. The scaffold degradation kinetics were modeled by non-linear least squares regression using a three-parameter logistic equation (Table 1).

163x117mm (300 x 300 DPI)

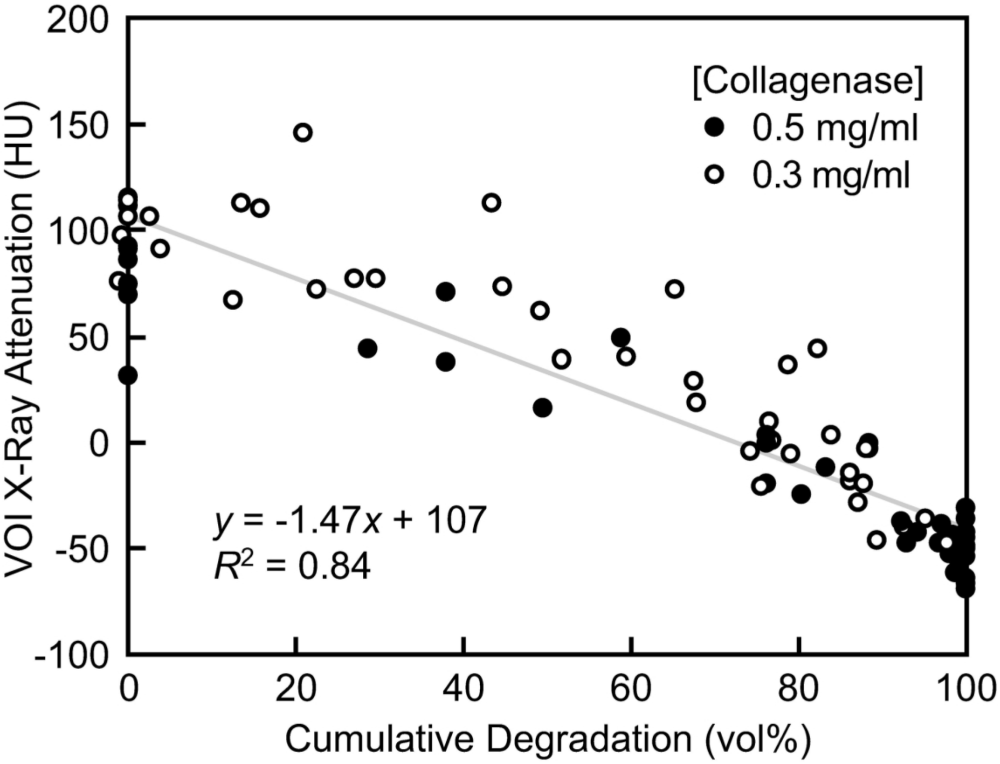

Fig. 6 The mean X-ray attenuation (HU) measured by micro-CT within a fixed VOI, including the entire volume of the media containing the scaffold and/or scaffold fragments, decreased linearly and was strongly correlated (R^2 = 0.84) with the cumulative degradation determined from the segmented scaffold volume in micro-CT. Note that the x-axis corresponds to all longitudinal measurements in Fig. 5a for enzymatic scaffold degradation in media containing 0.3 and 0.5 mg/ml collagenase. Measurements for media containing 0 mg/ml collagenase were omitted for clarity as these scaffolds did not exhibit degradation and all data points were thus clustered at approximately 0 vol% cumulative degradation and 100 HU.

166x127mm (300 x 300 DPI)

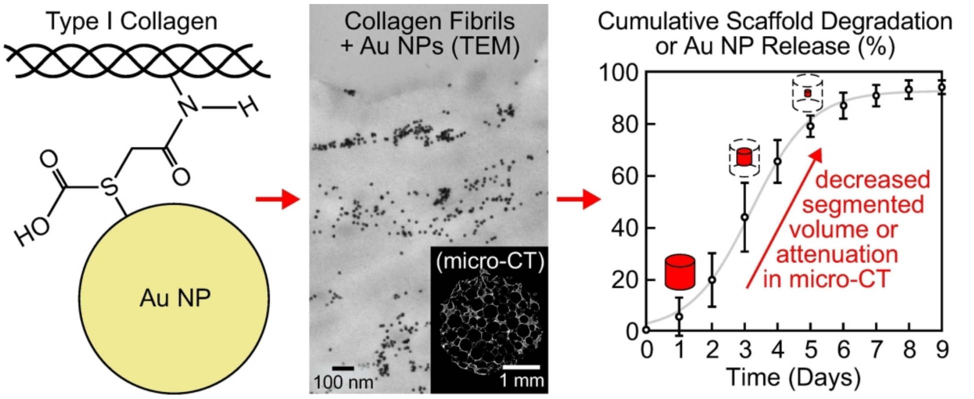

Gold nanoparticles and computed tomography were used synergistically to enable nondestructive, longitudinal, and volumetric measurement of collagen scaffold degradation.

170x83mm (300 x 300 DPI)